Resource

Cell Metabolism

Mitochondrial Transfer by Photothermal Nanoblade Restores Metabolite Profile in Mammalian Cells

Graphical Abstract

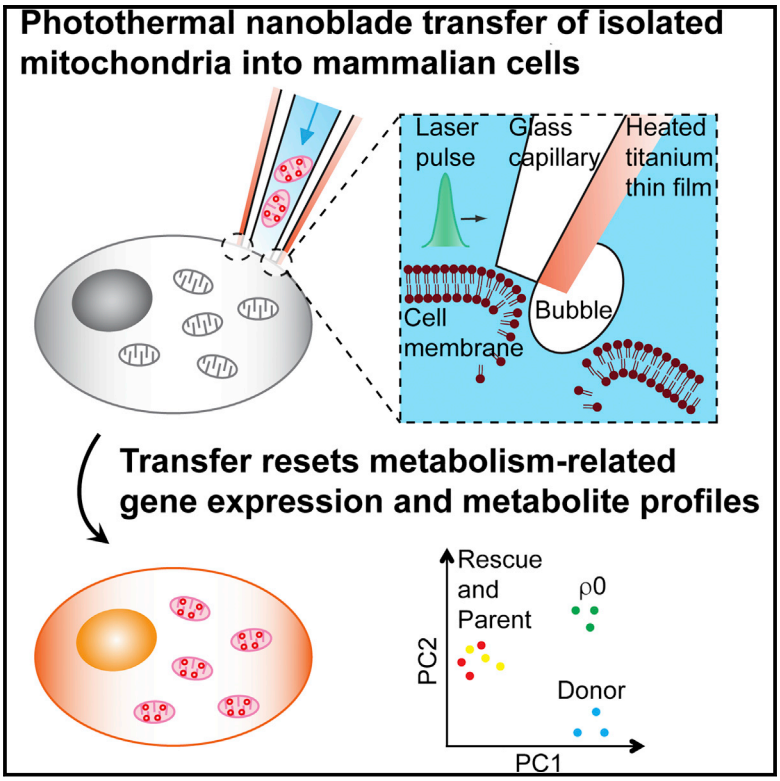

Authors

Ting-Hsiang Wu, Enrico Sagullo, Dana Case, ..., Thomas G. Graeber, Pei-Yu Chiou, Michael A. Teitell

Correspondence

pychiou@seas.ucla.edu (P.-Y.C.), mteitell@ucla.edu (M.A.T.)

In Brief

Optimizing mtDNA transfer into mammalian cells is an important step for basic studies and mitochondrial disease therapies. Using a photothermal nanoblade, Wu et al. are able to deliver isolated mitochondria into respiration-deficient cells. Rescued cell lines recover mitochondrial respiration and reset cellular metabolism to the parental cell level.

Highlights

- Proof-of-principle photothermal nanoblade transfer of mitochondria is reported
- Transfer into 143BTK− ρ0 cells generated rescue clones with recovered respiration
- Mitochondrial transfer reset metabolic enzyme gene expression patterns
- Two of three rescue clones showed metabolite profiles similar to 143BTK− parent cells

Wu et al., 2016, Cell Metabolism *23*, 921–929
May 10, 2016
http://dx.doi.org/10.1016/j.cmet.2016.04.007

Cell Metabolism
Resource

Mitochondrial Transfer by Photothermal Nanoblade Restores Metabolite Profile in Mammalian Cells

Ting-Hsiang Wu,[1,2,14,15] Enrico Sagullo,[1,14] Dana Case,[1,14] Xin Zheng,[1] Yanjing Li,[1] Jason S. Hong,[1] Tara TeSlaa,[3] Alexander N. Patananan,[1] J. Michael McCaffery,[4] Kayvan Niazi,[5,12,13] Daniel Braas,[6,7] Carla M. Koehler,[3,8,9,10] Thomas G. Graeber,[6,7,9,11,12] Pei-Yu Chiou,[2,12,13,*] and Michael A. Teitell[1,3,9,10,12,13,*]

[1]Department of Pathology and Laboratory Medicine, David Geffen School of Medicine, University of California, Los Angeles, Los Angeles, CA 90095, USA
[2]Department of Mechanical and Aerospace Engineering, University of California, Los Angeles, Los Angeles, CA 90095, USA
[3]Molecular Biology Institute, University of California, Los Angeles, Los Angeles, CA 90095, USA
[4]Integrated Imaging Center, Department of Biology, Johns Hopkins University, Baltimore, MD 21218, USA
[5]NantWorks, LLC, Culver City, CA 90232, USA
[6]Department of Molecular and Medical Pharmacology, David Geffen School of Medicine, University of California, Los Angeles, Los Angeles, CA 90095, USA
[7]UCLA Metabolomics Center, University of California, Los Angeles, Los Angeles, CA 90095, USA
[8]Department of Chemistry and Biochemistry, University of California, Los Angeles, Los Angeles, CA 90095, USA
[9]Jonsson Comprehensive Cancer Center, David Geffen School of Medicine, University of California, Los Angeles, Los Angeles, CA 90095, USA
[10]Eli and Edythe Broad Center of Regenerative Medicine and Stem Cell Research, University of California, Los Angeles, Los Angeles, CA 90095, USA
[11]Crump Institute for Molecular Imaging, David Geffen School of Medicine, University of California, Los Angeles, Los Angeles, CA 90095, USA
[12]California NanoSystems Institute, University of California, Los Angeles, Los Angeles, CA 90095, USA
[13]Department of Bioengineering, University of California, Los Angeles, Los Angeles, CA 90095, USA
[14]Co-first author
[15]Present address: NantWorks, LLC, Culver City, CA 90232, USA
*Correspondence: pychiou@seas.ucla.edu (P.-Y.C.), mteitell@ucla.edu (M.A.T.)
http://dx.doi.org/10.1016/j.cmet.2016.04.007

SUMMARY

mtDNA sequence alterations are challenging to generate but desirable for basic studies and potential correction of mtDNA diseases. Here, we report a new method for transferring isolated mitochondria into somatic mammalian cells using a photothermal nanoblade, which bypasses endocytosis and cell fusion. The nanoblade rescued the pyrimidine auxotroph phenotype and respiration of ρ0 cells that lack mtDNA. Three stable isogenic nanoblade-rescued clones grown in uridine-free medium showed distinct bioenergetics profiles. Rescue lines 1 and 3 reestablished nucleus-encoded anapleurotic and cataplerotic enzyme gene expression patterns and had metabolite profiles similar to the parent cells from which the ρ0 recipient cells were derived. By contrast, rescue line 2 retained a ρ0 cell metabolic phenotype despite growth in uridine-free selection. The known influence of metabolite levels on cellular processes, including epigenome modifications and gene expression, suggests metabolite profiling can help assess the quality and function of mtDNA-modified cells.

INTRODUCTION

Mitochondria are double-membrane eukaryotic organelles of α-proteobacterial origin (Sagan, 1967) that are maternally inherited and help produce energy (ATP) and intermediate metabolites, reducing agents (NADH and $FADH_2$), Fe-S clusters, heme, and steroids. They also generate reactive oxygen species during respiration and regulate apoptosis, Ca^{2+} homeostasis, and intracellular signaling (McBride et al., 2006). Mitochondria exist in an equilibrium between fused and fragmented morphologies that maintain their shape, size, number, and quality, and they contain their own non-nuclear genome (mtDNA) (Chan, 2012). In humans, the ~16.6 kb circular mtDNA encodes for 13 respiratory chain proteins, 22 tRNAs, and 2 rRNAs. Each nucleated cell contains a few to 100,000 copies of mtDNA that reside in nucleoids (García-Rodríguez, 2007). mtDNA mutations (http://www.mitomap.org/MITOMAP) can be silent or cause incurable familial diseases that affect high-energy tissues, including brain, heart, and muscle (Taylor and Turnbull, 2005). Cell dysfunction and disease may arise by a critical reduction in mtDNA number or by exceeding a threshold ratio between mutant and wild-type mtDNAs, creating a heteroplasmic state.

Unlike the nuclear genome, strategies for altering mtDNA are limited. Work to overcome the transmission of inherited mtDNA diseases has turned to preimplantation genetic diagnosis to evaluate risk. For women at risk, the transfer of the meiotic spindle-chromosomal complex or a polar body to a donor oocyte, or the transfer of pronuclei to a donor egg offers the potential for offspring with healthy mtDNA (Richardson et al., 2015). The generation of "three-parent" embryos as an assisted reproduction strategy has generated interest and debate, although these techniques cannot be used for somatic cells or after birth (Richardson et al., 2015; Vogel, 2014).

Alternative strategies for changing the mtDNA content in germ or somatic cells include somatic cell nuclear transfer (Ma et al., 2015; Tachibana et al., 2013) and manipulating the cellular heteroplasmy ratio. Heteroplasmy reduction through a "bottleneck" occurs naturally in early mammalian development and may occur with reprogramming somatic cells to pluripotency (Teslaa and Teitell, 2015). The bottleneck mechanism(s) for reducing heteroplasmy remain unresolved, and not all mtDNA haplotypes appear to survive. Mitochondrial targeted nucleases, including restriction endonucleases, zinc finger nucleases, and TALE nucleases, can enrich for specific mtDNAs by incomplete cleavage of target mtDNAs in a mixture, shifting the heteroplasmy ratio (Bacman et al., 2013).

The insertion or replacement of mtDNA sequences by genome editing tools or mitochondrial-targeted adeno-associated viruses (Yu et al., 2012) may also reduce specific mtDNA haplotypes. However, success for these procedures requires DNA repair by non-homologous end joining or homologous recombination, which occur infrequently in mammalian mitochondria (Alexeyev et al., 2013). Therefore, the acquisition of desired mtDNA haplotypes can only be accomplished by transferring mitochondria containing pre-existing mtDNAs into target cells. Successful approaches include cytoplasmic fusion between enucleated mitochondria donor cells and mtDNA eliminated ρ0 cells to generate transmitochondrial cybrid cell lines (Moraes et al., 2001). Also, direct microinjection of isolated mitochondria into somatic cells or oocytes (King and Attardi, 1988; Yang and Koob, 2012) and the transfer of isolated mitochondria, or mitochondrial transfer between cells, in vivo or in co-culture have been reported (Caicedo et al., 2015; Islam et al., 2012; Liu et al., 2014; Spees et al., 2006). However, microinjection is inefficient, and it remains unclear whether tunneling nanotube transfer or the "spontaneous" uptake of isolated mitochondria are general phenomena or condition/cell-type-specific mitochondrial transfer mechanisms.

Recently, we developed a photothermal nanoblade for efficient transfer of small and large objects into mammalian cells by direct cytoplasmic delivery (French et al., 2011; Wu et al., 2011, 2010). Here, we present a proof-of-principle study for nanoblade transfer of isolated mitochondria into ρ0 cells. Metabolomics analyses show the nanoblade is a controlled, reproducible, and general approach for changing the mtDNA haplotype in somatic mammalian cells and may be a potential first step toward reverse mitochondrial genetics.

RESULTS

Photothermal Nanoblade Configuration and Optimization

The apparatus consists of an inverted microscope with a 532 nm nanosecond pulsed laser that illuminates the field of view through the objective lens. A nanoblade delivery micropipette is mounted on a micromanipulator and connected to an external pressure source (Figures S1A and S1B). The micropipette tip is coated with a light-absorbing titanium thin-film ~100 nm thick (Wu et al., 2011, 2010). This coated tip is positioned to lightly touch the plasma membrane of a cell using the joystick controller. A transient membrane opening is induced by an ultrafast (<300 ns) and localized (<0.4 μm from micropipette rim) cavitation bubble, which forms from a laser pulse that rapidly heats the titanium thin film, causing vaporization of adjacent water layers in the culture media (Wu et al., 2011). Bubble expansion and collapse locally punctures the membrane and creates a several micron-long passageway for large cargo delivery that is rapidly repaired (Yamane et al., 2014). Pressure-driven fluid flow synchronized to the laser pulse transports cargo into the recipient cell cytosol. The micropipette does not penetrate the cell as in microinjection, is not sealed on the membrane, and membrane disruption is localized to the bubble nucleation site (Wu et al., 2010).

To deliver ~2 μm × 1 μm-sized mitochondria, the nanoblade was fabricated with a 3 μm bore tip inner diameter. This wide orifice prevents clogging and avoids excessive mitochondrial shearing (Figures S2A and S2B). The pulsed laser energy must surpass the superheating threshold for the nanoblade to generate a delivery portal without causing excessive damage and cell death. Optimization of plasma membrane opening efficiency and post-delivery cell viability is cell-type-specific and established by titration of the laser pulse fluence (mJ/cm^2) prior to mitochondria delivery (Wu et al., 2011, 2010). For 143BTK− ρ0 human osteosarcoma cells, a laser fluence of 108 mJ/cm^2 yields 64% membrane opening efficiency and 50% viability at 24 hr (Figure S2C). HeLa cells require 67% more laser energy (180 mJ/cm^2) for efficient membrane opening and 80% cell viability. Although photo-irradiation by laser illumination can depolarize mitochondria and cause their clearance by mitophagy (Kim and Lemasters, 2011), minimal to no loss of mitochondrial membrane potential (ΔΨ) occurred in isolated or whole-cell mitochondria, respectively, with repeated 108 mJ/cm^2 laser pulses (Figure S2D).

Mitochondrial Transfer

Recipient 143BTK− ρ0 cells were labeled with membrane potential-insensitive MitoTracker Green and seeded onto a 400 μm × 400 μm square on a patterned glass coverslip to simplify tracking (Figure 1A). HEK293T cells expressing mitochondria-targeted DsRed fluorescent protein (pMitoDsRed) were generated. ~0.5 mg/ml of isolated DsRed mitochondria were loaded into the nanoblade micropipette and delivered into ρ0 cells at ~100 cells/hr (Figure 1B). Confocal microscopy with z stack reconstruction showed donor DsRed and recipient MitoTracker Green-labeled mitochondria intermixed in the cytosol of recipient ρ0 cells 4 hr after delivery (Figure 1C).

MDA-MB-453 human breast carcinoma cells have genomic and mitochondrial DNA sequence polymorphisms and a unique MHC haplotype compared to 143BTK− ρ0 cells, providing distinguishing tags. Oxygen consumption rate (OCR) studies showed isolated mitochondria from 143BTK− parent and MDA-MB-453 cells respire, unlike 143BTK− ρ0 mitochondria (Figure 1D). Electron transport chain (ETC) coupling to oxidative phosphorylation (OXPHOS) expressed as the respiratory control ratio (RCR, state 3/state 4o respiration) provides an estimate of mitochondrial function. MDA-MB-453 and 143BTK− mitochondria had RCRs of 5.1 and 14.7, respectively, whereas 143BTK− ρ0 mitochondria had a negligible RCR.

ρ0 cells are pyrimidine auxotrophs that require uridine supplementation to grow because of an inactive dihydroorotate dehydrogenase (DHOD) enzyme resulting from a non-functional

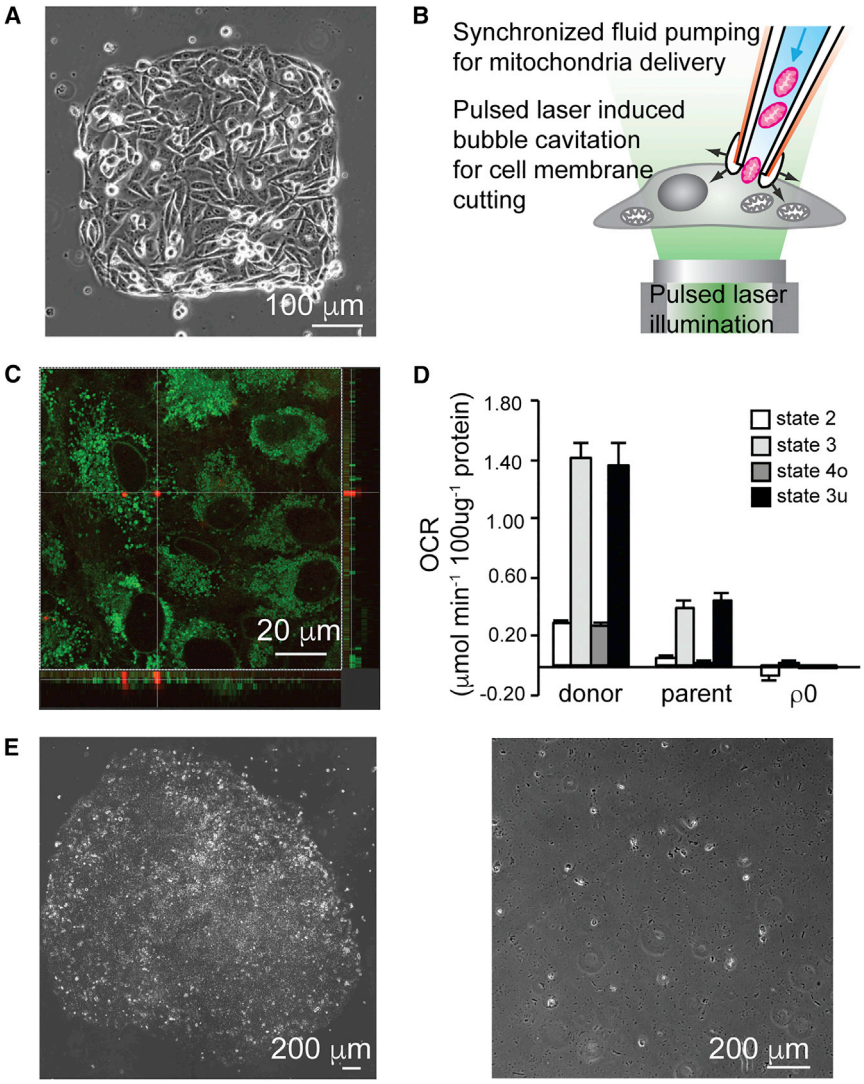

Figure 1. Generating Mitochondrial Rescue Clones by Photothermal Nanoblade

(A) Recipient 143BTK− ρ0 cells were seeded on a 400 μm × 400 μm square to facilitate nanoblade delivery, tracking, and clonal selection.

(B) Schematic of mitochondrial delivery by photothermal nanoblade. A 3 μm inner diameter glass microcapillary pipette tip coated externally with titanium is positioned to lightly contact the cell surface. A 532 nm pulsed laser illumination triggers a cavitation bubble to open the membrane with coordinated delivery of donor mitochondria into a cell using a fluid pump.

(C) Representative confocal image of two foci of DsRed-labeled donor mitochondria from HEK293T cells in the cytosol of a single 143BTK− ρ0 cell whose endogenous mitochondria are stained with MitoTracker Green (upper left quadrant).

(D) Isolated MDA-MB-453 donor and 143BTK− parent cell mitochondria remain functional and coupled. Mean ± SD (n = 3).

(E) 2 weeks post-nanoblade delivery, donor MDA-MB-453 (and 143BTK− parent, not shown) mitochondria transferred into 143BTK− ρ0 recipient cells generated "rescue" clones that emerged in uridine-free dialyzed media (left). 143BTK− ρ0 control cells (or 143BTK− ρ0 cells that received 143BTK− ρ0 donor mitochondria, not shown) died and detached from the plate when grown in uridine-free dialyzed media (right).

ETC (Grégoire et al., 1984). MDA-MB-453 mitochondria were loaded and nanoblade delivered into ~30 143BTK− ρ0 cells grown in uridine-added medium. 4 days post-delivery, cells were shifted to uridine-free medium, with the emergence of respiratory "rescue" clones starting at ~2 weeks (Figure 1E). The frequency of stable, rescue clone generation was 2.1% ± 3.1%, ~10-fold higher than microinjection (Table S1) (King and Attardi, 1988).

Clone Validation and Bioenergetic Analyses

Three nanoblade rescue clones were evaluated. Although ~15% of cells in rescue clones 2 and 3 had PicoGreen mtDNA staining after 2 weeks in uridine-free medium, >85% of cells in all three clones had mtDNA staining after 4 weeks (Figure 2A). Total DNA from donor, parent, ρ0 recipient, and clone 1–3 cells were PCR amplified with primers for mtDNA D-loop hypervariable control region (Figure 2B) and a single nucleotide polymorphism, rs2981582, in the nucleus-encoded *FGFR2* gene. Sequencing confirmed all three rescue clones contained exclusively donor mtDNA and ρ0 recipient genomic DNA (Figures 2C and 2D). MHC haplotype analysis showed rescue clone 1 contained the recipient cell nucleus (Figure 2E).

Rescue clones 1–3 proliferated at a similar rate to 143BTK− parent cells in uridine-free medium, suggesting the recovery of ETC and DHOD functions (Figure 3A). None of the lines proliferated in 2-deoxyglucose, which blocks glycolysis, but growth in galactose, which favors OXPHOS, was variable (Robinson, 1996), suggesting the clones were not metabolically equivalent. Steady-state ATP levels in clones 1 and 3 were at or above the donor and parent cell levels, respectively, but clone 2 had reduced ATP (Figure 3B). OCR showed basal, maximal respiration, and specific ETC complex I, II, and IV activities for clones 1 and 3 were similar to parent and donor lines, but clone 2 respiration was lower and ρ0 cell respiration absent (Figure 3C). Combined proliferation rate, ATP level, respiratory, and ETC complex activity data suggest rescue clones 1 and 3 are energetically distinct from clone 2 and more similar to the parent cells than to donor or ρ0 recipient cells. The data reveal a range of functional reconstitution by the nanoblade transfer of mitochondria and the restoration of transferred mtDNA.

A respiration-independent measure of mitochondrial biomass was provided by citrate synthase enzymatic activity (Zhang et al., 2011), which was similar between rescue clones 1–3, donor, recipient, and parent cells (Figure 3D). ρ0 recipient cells have a granular mitochondrial network (Margineantu et al., 2002) that is retained in rescue clone 1 cells (Figure S3A). Ultrastructure

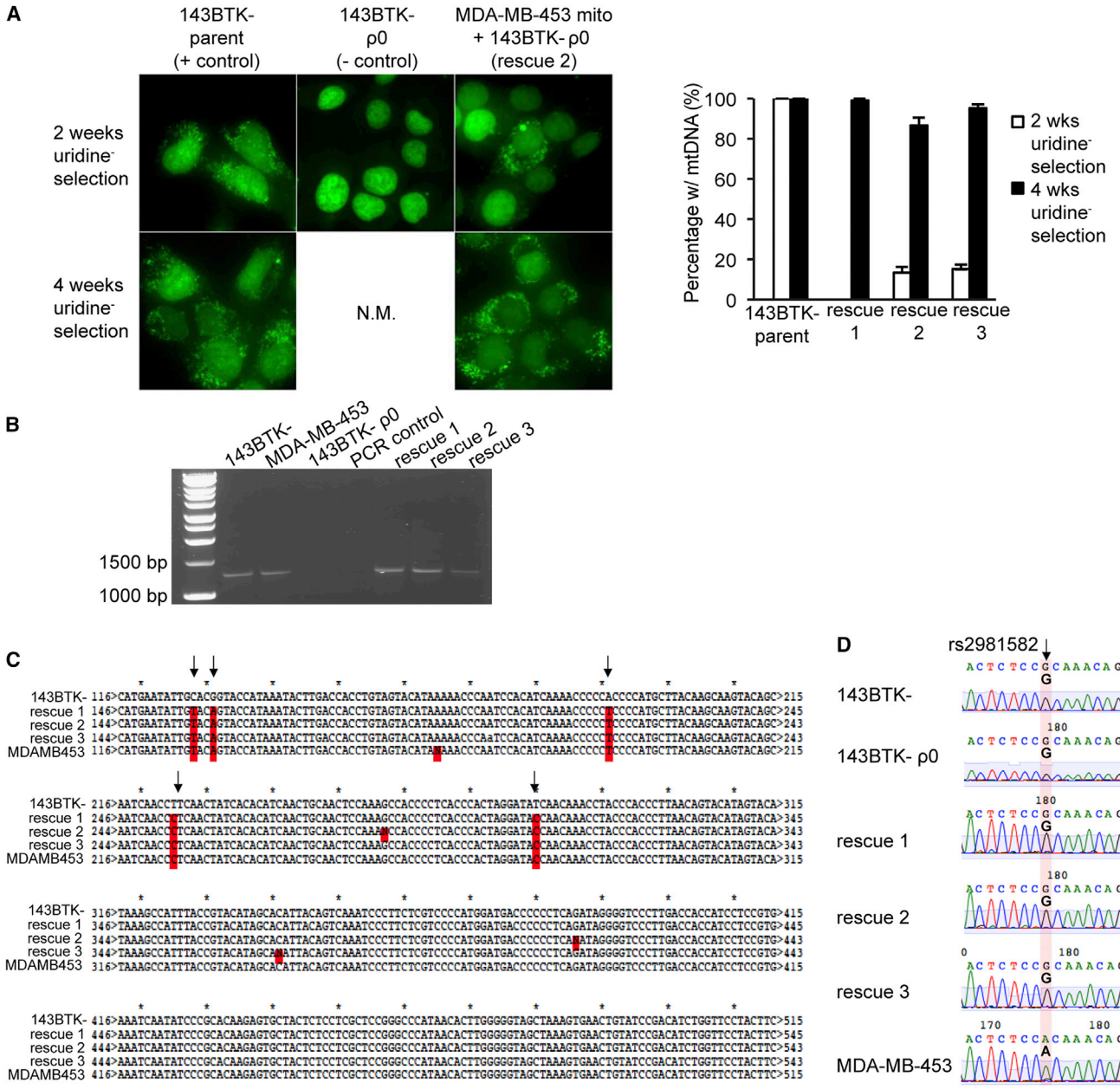

E

Cell line	DRB1 locus		A locus		B locus	
MDA-MB-453	03	13	01	01	08	08
143BTK- ρ0	15:02	16:02	02	02	52	52
rescue 1	15:02	16:02	02	02	52	52

Figure 2. Recipient gDNA–Donor mtDNA Pairing Validates Rescue Clones

(A) PicoGreen staining of mtDNA in the cytoplasm of 143BTK− ρ0 cells containing nanoblade-transferred MDA-MB-453 mitochondria at 2 (top row) and 4 (bottom row) weeks post-delivery. 143BTK− ρ0 cells lack mtDNA, do not survive for 4 weeks in uridine− medium, and show only nuclear staining. At 2 weeks in uridine− medium, ~15% of rescue clones 2 and 3 cells have mtDNA, which appear as green puncta in the cytoplasm. By 4 weeks of uridine− selection, >85% of cells in rescue clones 1–3 have mtDNA. Mean ± SD.

(B) PCR of mtDNA D-loop hypervariable region from rescue clones 1–3 with controls.

(C) Sequencing of mtDNA D-loop hypervariable region revealed multiple single nucleotide polymorphisms (SNPs, red color, arrows) present in rescue clones 1–3 and donor MDA-MB-453.

(legend continued on next page)

analysis by transmission electron microscopy showed that rescue clone 1 mitochondria had tightly stacked cristae with elevated electron density (Figures S3B–S3D). mtDNA levels by qPCR varied >10-fold between rescue clones 1–3 and did not correlate with proliferation rate, ATP level, OCR, or ETC complex activities (Figure 3E). Also, mitochondrial *ND1* and *ND2* transcript expression did not correlate with mtDNA content for clones 1–3, suggesting that differences in mtDNA expression are not the source of variable rescue quality or function (Figure 3F). Finally, $\Delta\Psi$ was quantified with tetramethylrhodamine methyl ester (TMRM). ρ0 cells hydrolyze ATP in mitochondria to maintain viability and showed a low $\Delta\Psi$ (Hatefi, 1985). Rescue clones 1 and 3 had fully restored $\Delta\Psi$ equivalent to parent cells, but rescue clone 2 showed $\Delta\Psi$ restoration in between the parent and ρ0 recipient cells (Figure 3G). Thus, $\Delta\Psi$ provided a potentially superior biomarker for mitochondrial function in rescue clones from nanoblade transfer.

Restoring Metabolism-Related Gene Expression

The introduction of mtDNA into ρ0 cells could affect nuclear gene expression directly, by impacting transcription factors, or indirectly, by changing metabolite levels that regulate signal transduction and epigenetics (Kaelin and McKnight, 2013; Teslaa and Teitell, 2015). Changes to nucleus-encoded gene expression patterns by rescuing ρ0 cells through the transfer of isolated mitochondria have not yet been assessed. Therefore, the steady-state expression of 33 genes encoding anapleurotic or catapleurotic enzymes was quantified by qRT-PCR (Figures S4A and S4B). An unbiased, systems-level assessment of steady-state gene expression was obtained by principle component analysis (PCA), which investigated relationships among all six cell lines (Figure 4A). Rescue clones 1 and 3 had gene expression profiles similar to the parent, whereas rescue clone 2 was similar to ρ0 recipient. Donor cells showed a distinct gene expression profile compared to the other cell lines. The data indicate that nanoblade transfer of mtDNA resets the nucleus-encoded metabolic enzyme gene expression pattern partially (clone 2) or almost completely (clones 1 and 3) to the parental, and not the donor, cell nucleus in an isogenic nuclear background.

Metabolite Profiling

Intracellular metabolite levels have not been quantified for mtDNA-modified systems. A liquid chromatography-mass spectrometry (LC/MS)-based metabolomics assay assessed TCA cycle-related and select cytosolic metabolites that could impact gene expression and cellular biosynthetic functions. Of 12 TCA cycle-related metabolites (sans pyruvate, whose quantification was highly variable), alpha-ketoglutarate (α-KG) and citrate (Cit) stood out as strongly depleted in ρ0 recipient cells compared to parent cells (Figure 4B). All three rescue clones showed increased α-KG and citrate above those in the ρ0 recipient. In contrast, ρ0 recipient cells accumulated the oncometabolite 2-hydroxyglutarate (2-HG) and succinate (Succ) relative to parent cells. All three rescue clones resolved the block at succinate dehydrogenase (ETC complex II), although clone 2 retained elevated 2-HG levels in contrast to clones 1 and 3. An unbiased assessment of 96 metabolites, including amino acids and nucleotides, was obtained by hierarchical clustering (Figure 4C) and PCA (Figure S4C) to evaluate the systems level rescue of ρ0 recipient cells by nanoblade. Rescue clones 1 and 3 clustered with parent cells, whereas rescue clone 2 grouped together with ρ0 recipient cells, and donor cells stood apart from both of these clusters. Similar to nucleus-encoded gene expression, nanoblade transfer of mtDNA restores the steady-state metabolite pattern of ρ0 recipient cells partially (clone 2) or almost completely (clones 1 and 3) to the parent and not the donor cells in an isogenic nuclear system.

The activities of metabolic pathways and the contributions of nutrients to specific intracellular metabolites were examined with stable isotope labeling. Fully labeled [U-^{13}C] glucose (Glc) and glutamine (Gln) provided the fractional contribution to network metabolites for recipient, parent, donor, and rescue clone 1–3 lines (Figure S4D). Rescue clones 1 and 3 grouped with the parent line by PCA, while rescue clone 2 was metabolically more similar to ρ0 recipient cells and the donor line was metabolically distinct from all other analyzed cell lines. Overall, the data suggested that gene expression, metabolic network activity, and metabolite levels in ρ0 recipient cells were almost completely restored to the parent cell levels in rescue clones 1 and 3, but not in rescue clone 2.

DISCUSSION

In a proof-of-principle study, we demonstrated that the photothermal nanoblade can transfer isolated mitochondria from an allogeneic cell type to restore metabolic gene expression, global energetic, and metabolite profiles. The nanoblade enables comparisons of different mitochondria and their metabolic performance in an isogenic nuclear background. The mtDNA level, mtRNA expression, mitochondrial biomass, and ultrastructure did not correlate with rescue clone performance. A broad range of rescue clone respiration and respiratory capacity unrelated to mtDNA or mtRNA levels was also reported for clones previously generated via microinjection (King and Attardi, 1989) and cybrid fusion (Chomyn et al., 1994). Instead, system-wide activities as reflected by $\Delta\Psi$ and global metabolite recovery were a better predictor of rescue clone quality and function. Hierarchical clustering and PCA of steady-state metabolite levels and the fractional contribution of glucose and glutamine to isotopologues indicate that rescue clones 1 and 3 are restored to the parental metabolic profile. Interestingly, the partially rescued clone 2 survived uridine-free selection and still remained most similar to ρ0 cells, possibly by sufficient recovery of ETC function to increase DHOD activity and uridine production. This idea is supported from the reversal of the ETC complex II (succinate dehydrogenase) block and full recovery of parent succinate levels for all three rescue clones. All three rescue clones adopted features of the recipient and not the donor.

(D) Rescue clones 1–3 contained the same SNP in the *FGFR2* nuclear gene as 143BTK− parent and 143BTK− ρ0 cells (arrow), but a distinct SNP from mitochondrial donor MDA-MB-453 cells.

(E) Human leukocyte antigen (HLA) analysis of rescue 1 shows the same major histocompatibility complex (MHC) loci as 143BTK− parent and 143BTK− ρ0 cells.

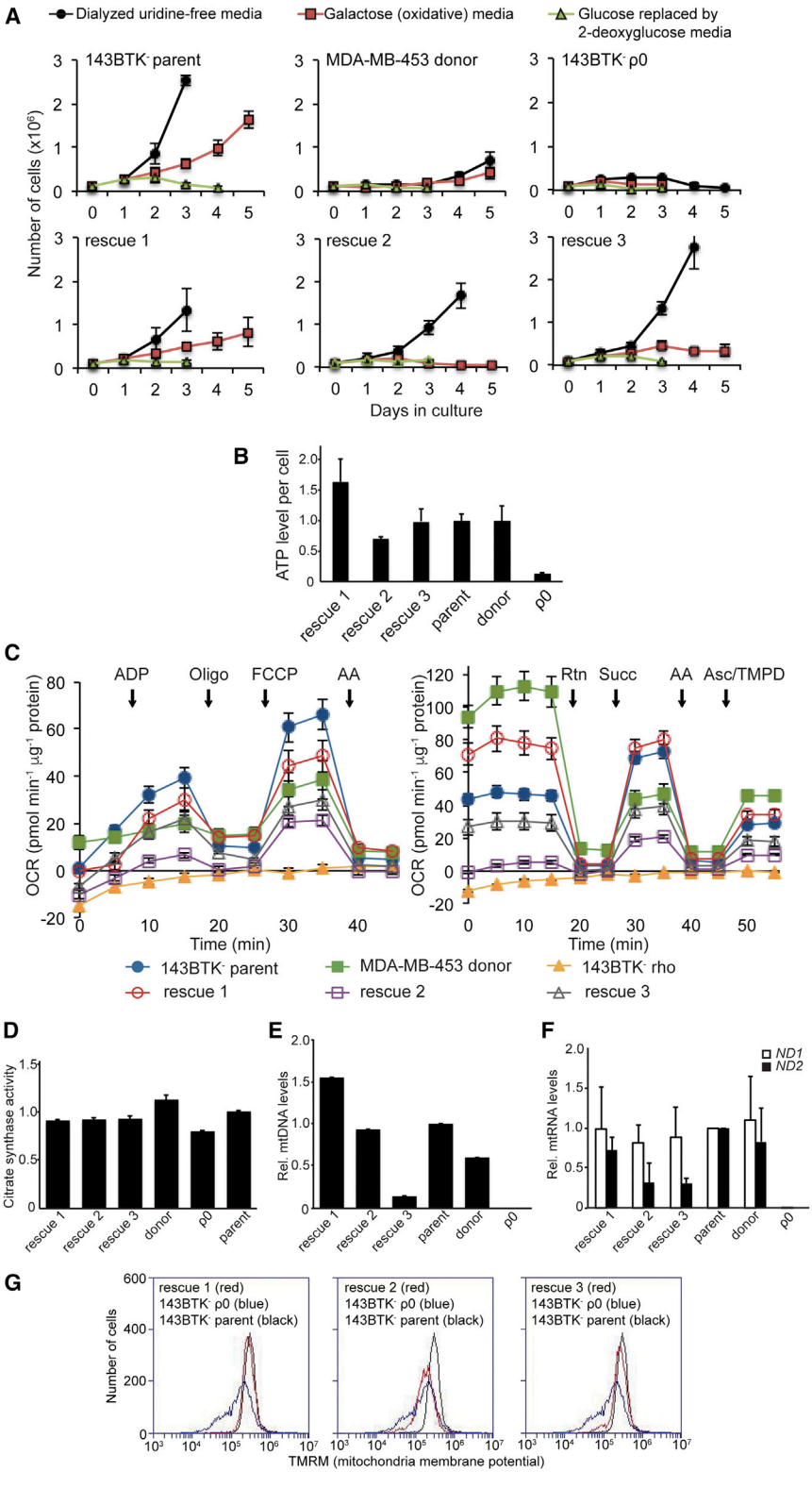

Figure 3. Bioenergetic Profile of Rescue Clones

(A) Proliferation of 143BTK− parent, MDA-MB-453 donor, 143BTK− ρ0, and rescue clone 1–3 cells in the indicated media formulations. Mean ± SD (n = 3).

(B) Steady-state intracellular ATP levels in arbitrary units. Mean ± SD (n = 3).

(C) Mitochondria coupling assay (left) and electron flow assay (right) as measured by Seahorse XF24 Analyzer. Mean ± SD (n = 3).

(D) Ratio of citrate synthase enzyme activity to total cellular protein, normalized to 1.0 for the 143BTK− parent line. Mean ± SD (n = 3).

(E) mtDNA quantification by qPCR, normalized to 1.0 for the 143BTK− parent line. Mean ± SD (n = 3).

(F) mtDNA-encoded *ND1* and *ND2* transcript quantification by qRT-PCR, normalized to 1.0 for the 143BTK− parent line. Mean ± SD (n = 3).

(G) Representative mitochondrial membrane potential quantified by TMRM staining and flow cytometry.

molecules. Initial applications for the nanoblade approach include more detailed studies of mtDNA expansion kinetics with or without manipulations of regulators of mtDNA replication or mitochondrial fusion/fission. A defined ratio of mixed donor mitochondria can also be simultaneously transferred into a cell, which aids in studies of heteroplasmy mtDNA competition, nuclear/mitochondrial genome compatibility, and kinetics of metabolic rewiring. Finally, the nanoblade could dissect mechanisms of inefficient, uncontrolled, and spontaneous cellular uptake of mitochondria without cell fusion (Katrangi et al., 2007; Kitani et al., 2014; Masuzawa et al., 2013).

Mitochondria transfer by photothermal nanoblade is ~2% efficient, which is higher than cell fusion (0.0001%–0.5%) (Tables S2 and S3). However, the nanoblade is low throughput because mitochondria are transferred into successive individual cells. Due to variable recovery of recipient cell function seen with all reported mitochondrial transfer approaches, a larger number of clones in each experiment are needed to obtain a spectrum of clone performance and enable the selection of optimal clones for a particular purpose. A potential solution is the recent development of a biophotonic laser-assisted surgery tool (BLAST) for the massively parallel transfer of large cargo into mammalian cells using the same biophysical principle as the one-cell-at-a-time nanoblade, with appropriate modifications and optimization for mitochondrial transfer reactions (Wu et al., 2015).

Compared to cell fusion, the photothermal nanoblade can deliver washed, isolated mitochondria, minimizing the transfer of other cytosolic biomolecules that could impact biological functions in cells, such as microRNAs, metabolites, and signaling

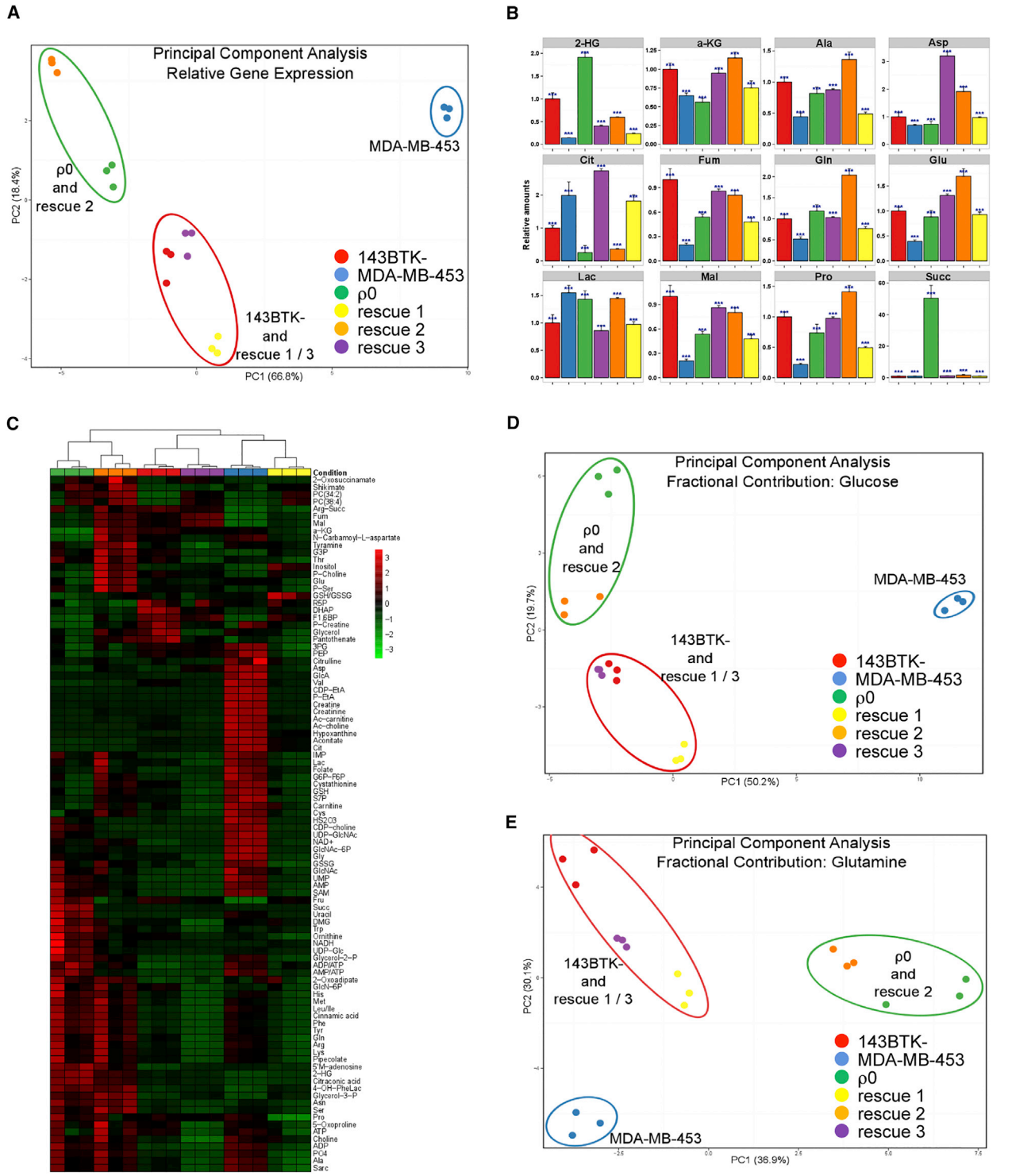

Figure 4. Metabolic Gene Expression and Metabolite Profile of Rescue Clones

(A) Expression of 33 genes involved in TCA cycle metabolism quantified by qRT-PCR and normalized to the ribosomal *36B4* gene (see Figure S4B). PCA shows the grouped relationships between the six cell lines studied.

(B) Relative levels of 12 TCA cycle proximate metabolites quantified by LC-MS/MS and normalized to the 143BTK− parental line. Mean ± SD (n = 3). Color code consistent with rest of sub-figures.

(C) Heatmap of 96 metabolites measured with an ANOVA p value equal to or less than 0.05. Samples were clustered using a Pearson correlation matrix.

(D) PCA using the fractional contribution from U-^{13}C glucose to all measured metabolites.

(E) PCA using the fractional contribution from U-^{13}C glutamine to all measured metabolites.

EXPERIMENTAL PROCEDURES

Standard procedures were followed for cell culture, sequencing, oxygen consumption studies, ATP quantification, microscopy, citrate synthase and $\Delta\Psi$ assays, qPCR and qRT-PCR, and metabolomics, as described in the Supplemental Experimental Procedures.

Photothermal Nanoblade

Borosilicate glass micropipettes with a tip ~3 μm in diameter and ~5 mm long were generated using a micropipette puller (Sutter Instrument, P-97). An ~100 nm titanium thin film was deposited on the tip and outer walls of pulled micropipettes using a magnetron sputterer deposition system (Denton Vacuum, Discovery 550).

Photothermal Nanoblade Operation and Optimization

The photothermal nanoblade delivery system (Figures S1A and S1B) uses an inverted microscope (Zeiss, AxioObserver) anchored to an optical table equipped with vibration damping control (Newport, RS Series). A 40× 0.6 NA objective lens was used to view target cell-micropipette tip placement and to channel a pulsed laser beam onto the sample plane. The laser is a Q-switched, frequency-doubled Nd:YAG laser (Continuum, Minilite) with a linearly polarized laser pulse output at 532 nm in wavelength and 6 ns in pulse width. A half wave plate (Newport, 10RP12-16) and a polarizing beam splitter (Newport, 05BC15PH.3) were installed in the laser beam path to adjust the laser energy. The beam was aligned into the epi-fluorescence port of the microscope and reflected into the back aperture of the objective lens onto the sample plane by a dichroic mirror (Chroma, Z532RDC). A long-pass filter (Chroma, HQ570LP) was used to block any back-scattered light from reaching an imaging camera (Hamamatsu, ORCA). An optical diffuser (Edmund Optics, NT55-848) and two convex lenses, f1 = 25 mm and f2 = 60 mm, were placed in the beam path to smoothen the laser intensity profile and to control the dimension of the laser spot size at the sample/imaging plane. The laser spot diameter at the imaging plane was 260 μm and covered the entire field of view. A motorized micromanipulator (Eppendorf, InjectMan NI 2) was mounted adjacent to the microscope stage to enable positioning of the titanium-coated micropipette tip using a joystick. A programmable pressure source (Eppendorf, Femtojet) drove liquid and suspended mitochondria into cells. A double pole, single throw switch (Digi-Key, P8101S-ND) was used to coordinately trigger laser pulsing and Femtojet delivery activities.

To optimize the laser intensity for mitochondria delivery, fluorescent dextran (200 μg/ml in 1× PBS [pH 7.4]) (Invitrogen, D-3305) was delivered into 20–30 cells at each laser power spanning a range from 72 to 216 mJ/cm^2. Cell membrane opening efficiency was scored as the number of fluorescent cells divided by the number of delivered cells (Figure S2C). Cell viability was determined as the number of dextran-containing cells that exclude propidium iodide out of the total number of delivered cells at 2 hr post-nanoblade delivery. The compensation pressure (pc) was set to 5 hPa on the Femtojet so that a trace amount of fluorescent dye discharged from the tip. The injection pressure (pi) was set to 15 hPa, and injection time (ti) was ~0.1 s to minimize cell lysis from the delivered fluid volume.

Mitochondrial Isolation and Delivery

Mitochondria isolation was performed using standard methods (Frezza et al., 2007). Briefly, MDA-MB-453 cells were detached from an 80%–90% confluent 15 cm petri dish using a cell scraper and suspended in 1 ml ice-cold isolation buffer, IB_c (10 mM Tris/MOPS, 5 mM EGTA/Tris and 0.2 M sucrose, 1 mM protease inhibitor [Sigma, P8340] and 0.2% BSA, adjusted to pH 7.4). Cell suspension was homogenized using a Teflon pestle in a glass potter with 30 strokes on ice and the mitochondrial fraction obtained after centrifugation washes. Isolated mitochondria pellet was resuspended in ice-cold experimental buffer, EB_c (125 mM KCl, 10 mM Tris/MOPS, 1 mM EGTA/Tris, 0.1 M sucrose, 1 mM KH_2PO_4, 1 mM protease inhibitor, and 0.2% BSA, adjusted to pH 7.4). Resuspended mitochondria (0.5 mg/ml protein concentration) were kept on ice until delivery. ~8 μl of isolated mitochondria suspension was loaded into a nanoblade micropipette. Nanoblade deliveries were done into ~30 cells per experiment (Table S1), and successful delivery was visualized by transient cytosol volume expansion.

Statistical Analysis

Experiments were carried out in triplicate, and data represent the mean ± SD. Student's t test was used to determine p values.

SUPPLEMENTAL INFORMATION

Supplemental Information includes Supplemental Experimental Procedures, four figures, and three tables and can be found with this article online at http://dx.doi.org/10.1016/j.cmet.2016.04.007.

AUTHOR CONTRIBUTIONS

T.-H.W. and E.S. engineered the photothermal nanoblade platform. T.-H.W., E.S., D.C., X.Z., J.S.H., A.N.P., J.M.M., and K.N. generated mitochondrial rescue cell lines and molecular and cellular data. Y.L., T.T., D.B., and T.G.G. generated and analyzed metabolite profiling data. T.-H.W., C.M.K., P.-Y.C., and M.A.T. designed the research and/or analyzed data with help from all other authors. T.-H.W. and M.A.T. wrote the paper with help from E.S., D.C., D.B., C.M.K., and P.-Y.C.

ACKNOWLEDGMENTS

We were supported by UC Discovery Biotechnology grant 178517, Air Force Office of Scientific Research grant FA9550-15-1-0406, NIH grants GM007185, GM114188, GM073981, GM061721, EB014456, CA009056, CA90571, CA009120, CA156674, CA185189, and CA168585, NSF grant CBET-1404080, CIRM grants RB1-01397 and RT3-07678, Prostate Cancer Foundation Challenge Award, Broad Stem Cell Research Center Training Grant and Innovator Award, American Cancer Society Research Scholar Award RSG-12-257-01-TBE, Melanoma Research Alliance Established Investigator Award 20120279, National Center for Advancing Translational Sciences UCLA CTSI Grant UL1TR000124, and NanoCav, LLC. The authors thank S. Rabizadeh (Nantworks, LLC) for helpful discussions and support. T.-H.W. and K.N. are employees of NantWorks, LLC, which has licensed the rights to the photothermal nanoblade from the University of California, Los Angeles. P.-Y.C. and M.A.T. receive sponsored research funding from NantWorks, LLC.

Received: November 3, 2015
Revised: February 10, 2016
Accepted: April 12, 2016
Published: May 10, 2016

REFERENCES

Alexeyev, M., Shokolenko, I., Wilson, G., and LeDoux, S. (2013). The maintenance of mitochondrial DNA integrity–critical analysis and update. Cold Spring Harb. Perspect. Biol. *5*, a012641.

Bacman, S.R., Williams, S.L., Pinto, M., Peralta, S., and Moraes, C.T. (2013). Specific elimination of mutant mitochondrial genomes in patient-derived cells by mitoTALENs. Nat. Med. *19*, 1111–1113.

Caicedo, A., Fritz, V., Brondello, J.M., Ayala, M., Dennemont, I., Abdellaoui, N., de Fraipont, F., Moisan, A., Prouteau, C.A., Boukhaddaoui, H., et al. (2015). MitoCeption as a new tool to assess the effects of mesenchymal stem/stromal cell mitochondria on cancer cell metabolism and function. Sci. Rep. *5*, 9073.

Chan, D.C. (2012). Fusion and fission: interlinked processes critical for mitochondrial health. Annu. Rev. Genet. *46*, 265–287.

Chomyn, A., Lai, S.T., Shakeley, R., Bresolin, N., Scarlato, G., and Attardi, G. (1994). Platelet-mediated transformation of mtDNA-less human cells: analysis of phenotypic variability among clones from normal individuals–and complementation behavior of the tRNALys mutation causing myoclonic epilepsy and ragged red fibers. Am. J. Hum. Genet. *54*, 966–974.

French, C.T., Toesca, I.J., Wu, T.H., Teslaa, T., Beaty, S.M., Wong, W., Liu, M., Schröder, I., Chiou, P.Y., Teitell, M.A., and Miller, J.F. (2011). Dissection of the Burkholderia intracellular life cycle using a photothermal nanoblade. Proc. Natl. Acad. Sci. USA *108*, 12095–12100.

Frezza, C., Cipolat, S., and Scorrano, L. (2007). Organelle isolation: functional mitochondria from mouse liver, muscle and cultured fibroblasts. Nat. Protoc. *2*, 287–295.

García-Rodríguez, L.J. (2007). Appendix 1. Basic properties of mitochondria. Methods Cell Biol. *80*, 809–812.

Grégoire, M., Morais, R., Quilliam, M.A., and Gravel, D. (1984). On auxotrophy for pyrimidines of respiration-deficient chick embryo cells. Eur. J. Biochem. *142*, 49–55.

Hatefi, Y. (1985). The mitochondrial electron transport and oxidative phosphorylation system. Annu. Rev. Biochem. *54*, 1015–1069.

Islam, M.N., Das, S.R., Emin, M.T., Wei, M., Sun, L., Westphalen, K., Rowlands, D.J., Quadri, S.K., Bhattacharya, S., and Bhattacharya, J. (2012). Mitochondrial transfer from bone-marrow-derived stromal cells to pulmonary alveoli protects against acute lung injury. Nat. Med. *18*, 759–765.

Kaelin, W.G., Jr., and McKnight, S.L. (2013). Influence of metabolism on epigenetics and disease. Cell *153*, 56–69.

Katrangi, E., D'Souza, G., Boddapati, S.V., Kulawiec, M., Singh, K.K., Bigger, B., and Weissig, V. (2007). Xenogenic transfer of isolated murine mitochondria into human rho0 cells can improve respiratory function. Rejuvenation Res. *10*, 561–570.

Kim, I., and Lemasters, J.J. (2011). Mitophagy selectively degrades individual damaged mitochondria after photoirradiation. Antioxid. Redox Signal. *14*, 1919–1928.

King, M.P., and Attardi, G. (1988). Injection of mitochondria into human cells leads to a rapid replacement of the endogenous mitochondrial DNA. Cell *52*, 811–819.

King, M.P., and Attardi, G. (1989). Human cells lacking mtDNA: repopulation with exogenous mitochondria by complementation. Science *246*, 500–503.

Kitani, T., Kami, D., Matoba, S., and Gojo, S. (2014). Internalization of isolated functional mitochondria: involvement of macropinocytosis. J. Cell. Mol. Med. *18*, 1694–1703.

Liu, K., Ji, K., Guo, L., Wu, W., Lu, H., Shan, P., and Yan, C. (2014). Mesenchymal stem cells rescue injured endothelial cells in an in vitro ischemia-reperfusion model via tunneling nanotube like structure-mediated mitochondrial transfer. Microvasc. Res. *92*, 10–18.

Ma, H., Folmes, C.D., Wu, J., Morey, R., Mora-Castilla, S., Ocampo, A., Ma, L., Poulton, J., Wang, X., Ahmed, R., et al. (2015). Metabolic rescue in pluripotent cells from patients with mtDNA disease. Nature *524*, 234–238.

Margineantu, D.H., Gregory Cox, W., Sundell, L., Sherwood, S.W., Beechem, J.M., and Capaldi, R.A. (2002). Cell cycle dependent morphology changes and associated mitochondrial DNA redistribution in mitochondria of human cell lines. Mitochondrion *1*, 425–435.

Masuzawa, A., Black, K.M., Pacak, C.A., Ericsson, M., Barnett, R.J., Drumm, C., Seth, P., Bloch, D.B., Levitsky, S., Cowan, D.B., and McCully, J.D. (2013). Transplantation of autologously derived mitochondria protects the heart from ischemia-reperfusion injury. Am. J. Physiol. Heart Circ. Physiol. *304*, H966–H982.

McBride, H.M., Neuspiel, M., and Wasiak, S. (2006). Mitochondria: more than just a powerhouse. Curr. Biol. *16*, R551–R560.

Moraes, C.T., Dey, R., and Barrientos, A. (2001). Transmitochondrial technology in animal cells. Methods Cell Biol. *65*, 397–412.

Richardson, J., Irving, L., Hyslop, L.A., Choudhary, M., Murdoch, A., Turnbull, D.M., and Herbert, M. (2015). Concise reviews: Assisted reproductive technologies to prevent transmission of mitochondrial DNA disease. Stem Cells *33*, 639–645.

Robinson, B.H. (1996). Use of fibroblast and lymphoblast cultures for detection of respiratory chain defects. Methods Enzymol. *264*, 454–464.

Sagan, L. (1967). On the origin of mitosing cells. J. Theor. Biol. *14*, 255–274.

Spees, J.L., Olson, S.D., Whitney, M.J., and Prockop, D.J. (2006). Mitochondrial transfer between cells can rescue aerobic respiration. Proc. Natl. Acad. Sci. USA *103*, 1283–1288.

Tachibana, M., Amato, P., Sparman, M., Gutierrez, N.M., Tippner-Hedges, R., Ma, H., Kang, E., Fulati, A., Lee, H.S., Sritanaudomchai, H., et al. (2013). Human embryonic stem cells derived by somatic cell nuclear transfer. Cell *153*, 1228–1238.

Taylor, R.W., and Turnbull, D.M. (2005). Mitochondrial DNA mutations in human disease. Nat. Rev. Genet. *6*, 389–402.

Teslaa, T., and Teitell, M.A. (2015). Pluripotent stem cell energy metabolism: an update. EMBO J. *34*, 138–153.

Vogel, G. (2014). Assisted reproduction. FDA considers trials of 'three-parent embryos'. Science *343*, 827–828.

Wu, T.H., Teslaa, T., Teitell, M.A., and Chiou, P.Y. (2010). Photothermal nanoblade for patterned cell membrane cutting. Opt. Express *18*, 23153–23160.

Wu, T.H., Teslaa, T., Kalim, S., French, C.T., Moghadam, S., Wall, R., Miller, J.F., Witte, O.N., Teitell, M.A., and Chiou, P.Y. (2011). Photothermal nanoblade for large cargo delivery into mammalian cells. Anal. Chem. *83*, 1321–1327.

Wu, Y.C., Wu, T.H., Clemens, D.L., Lee, B.Y., Wen, X., Horwitz, M.A., Teitell, M.A., and Chiou, P.Y. (2015). Massively parallel delivery of large cargo into mammalian cells with light pulses. Nat. Methods *12*, 439–444.

Yamane, D., Wu, Y.C., Wu, T.H., Toshiyoshi, H., Teitell, M.A., and Chiou, P.Y. (2014). Electrical impedance monitoring of photothermal porated mammalian cells. J. Lab. Autom. *19*, 50–59.

Yang, Y.W., and Koob, M.D. (2012). Transferring isolated mitochondria into tissue culture cells. Nucleic Acids Res. *40*, e148.

Yu, H., Koilkonda, R.D., Chou, T.H., Porciatti, V., Ozdemir, S.S., Chiodo, V., Boye, S.L., Boye, S.E., Hauswirth, W.W., Lewin, A.S., and Guy, J. (2012). Gene delivery to mitochondria by targeting modified adenoassociated virus suppresses Leber's hereditary optic neuropathy in a mouse model. Proc. Natl. Acad. Sci. USA *109*, E1238–E1247.

Zhang, J., Khvorostov, I., Hong, J.S., Oktay, Y., Vergnes, L., Nuebel, E., Wahjudi, P.N., Setoguchi, K., Wang, G., Do, A., et al. (2011). UCP2 regulates energy metabolism and differentiation potential of human pluripotent stem cells. EMBO J. *30*, 4860–4873.